

Polymyxin B Loosens Lipopolysaccharide Bilayer but Stiffens Phospholipid Bilayer

Lei Fu,¹ Mingwei Wan,¹ Shan Zhang,¹ Lianghui Gao,^{1,*} and Weihai Fang¹

¹Key Laboratory of Theoretical and Computational Photochemistry, Ministry of Education, College of Chemistry, Beijing Normal University, Beijing, China

ABSTRACT Multidrug-resistant Gram-negative bacteria have increased the prevalence of a variety of serious diseases in modern times. Polymyxins are used as the last-line therapeutic options for the treatment of infections. However, the mechanism of action of polymyxins remains in dispute. In this work, we used a coarse-grained molecular dynamics simulation to investigate the mechanism of the cationic antimicrobial peptide polymyxin B (PmB) interacting with both the inner and outer membrane models of bacteria. Our results show that the binding of PmB disturbs the outer membrane by displacing the counterions, decreasing the orientation order of the lipopolysaccharide tail, and creating more lipopolysaccharide packing defects. Upon binding onto the inner membrane, in contrast to the traditional killing mechanism that antimicrobial peptides usually use to induce holes in the membrane, PmBs do not permeabilize the inner membrane but stiffen it by filling up the lipid packing defect, increasing the lipid tail order and the membrane bending rigidity as well as restricting the lipid diffusion. PmBs also mediate inter-membrane contact and adhesion. These joint effects suggest that PmBs deprive the biological activity of Gram-negative bacteria by sterilizing the cell.

SIGNIFICANCE The longstanding and unexplained puzzle of the antibacterial mechanism of polymyxin B on the inner and outer membranes of Gram-negative bacteria was studied by molecular dynamics simulations at coarse-grained resolution. We depicted the pathway of how polymyxins kill the Gram-negative bacteria: they soften and permeate across the outer membrane by releasing linker counterions between lipopolysaccharide molecules and then bind onto and stiffen the inner membrane by filling the phospholipid packing vacancy and restricting lipid diffusion, or they induce adhesion and lipid exchange between two phospholipid surfaces of the outer and inner membrane via bidirectional electrostatic and hydrophobic attraction and finally sterilize the bacterial cell. These findings may contribute to the development of therapeutic agents targeting bacteria.

INTRODUCTION

The prevalence of multidrug-resistant (MDR) Gram-negative bacteria has emerged as a major global public health crisis. However, relatively few novel antibiotic therapeutic compounds have been introduced to treat MDR bacteria in recent years. A promising solution to this crisis comes from antimicrobial peptides (AMPs), which are small, naturally existing proteins possessing considerable antibiotic properties. They are indispensable for defending animal and plant organisms from bacterial and viral infections. Since the first report of cecropins as cationic AMPs in early 1980, thousands of AMPs have been discovered and documented. These

AMPs have high diversity in their sequence composition, length, and secondary structure. Most AMPs act as broad-spectrum antibiotics by damaging the bacterial membrane via forming holes, and some can even translocate across the cell membrane and bind with intracellular DNA or RNA to prevent intracellular synthesis. The difficulty of bacteria to develop resistance to these AMPs makes them attractive as possible next-generation antimicrobial drugs to combat the growing global threat of multidrug antibiotic resistance. Polymyxin, a typical clinical AMP, is increasingly being used as the last-line therapy to treat infections caused by Gram-negative bacteria that are resistant to essentially all other currently available antibiotics (1–5).

There are two types of polymyxins available for clinical use: colistin (i.e., polymyxin E) and polymyxin B (PmB). Colistin and PmB share a common primary sequence and differ only at one residue, which is occupied by D-Phe in

Submitted August 28, 2019, and accepted for publication November 8, 2019.

*Correspondence: lhgao@bnu.edu.cn

Editor: Alan Grossfield.

<https://doi.org/10.1016/j.bpj.2019.11.008>

© 2019 Biophysical Society.

PmB but D-Leu in colistin. The two polymyxins both have a central structure of a linear trilipopeptide, one end of which connects to a cyclic heptapeptide, whereas the other connects to a fatty acid tail. Each residue of five L- α - γ -diaminobutyric acids (Dab) carries a charge of +1 (6). Since being discovered in the 1940s (7–9), polymyxin B and E have been subjected to contemporary drug-development procedures. They have a narrow antibacterial spectrum mainly against Gram-negative bacteria. The clinical use of colistin and PmB waned in the 1970s because of the early experience of nephrotoxicity and neurotoxicity after intravenous administration. Nevertheless, because no new antibiotics are available against the MDR Gram-negative “superbugs” currently as well as in the near future, polymyxins will continue to be used as the last-line therapeutic options for treatment of infections. In late 2015, the first example of a transferrable polymyxin resistance mechanism in Gram-negative pathogens, MCR-1, was reported, posing an enormous challenge to the use of polymyxin as a reserved drug for treatment of infections (10). It has led to a volcanic upsurge of research on how to reduce nephrotoxicity (11,12), modify residues to design polymyxin analogies (13), explore the antibiotic adjuvant to enhance the potency of colistin (14), and improve the activity of polymyxin in resistant bacteria (11,15). Meanwhile, it has sparked a worldwide research boom to investigate the bactericidal mechanism of polymyxins.

Although a number of models have been proposed based on experimental and theoretical researches, the action mechanism of polymyxins still remains in dispute. Some experiments found membrane blebbing (16) and electrochemical transmembrane potential dissipation in cells (17), which suggests that inner membrane (IM) permeabilization leads to bacterial cell death. To explain polymyxins’ rapid and concentration-dependent bacterial killing mechanism with negligible postantibiotic effects, Hancock et al. (18–22) proposed a general “self-promoted uptake” model. The model suggests that the aggregation of PmB promotes its own uptake across the outer membrane (OM) and subsequent pore formation of the IM. An alternative proposed mechanism is that PmB promotes vesicle-vesicle contacts and induces lipid exchange without leakage or fusion (23–25). This model suggests that PmB specifically targets Gram-negative bacteria by triggering contact formation between the two phospholipid interfaces in the periplasmic space (23). A third possible mechanism is based on a generalized mechanism for bactericidal agents in which an oxidative burst produces a reactive hydroxyl radical ($\cdot\text{OH}$) that can induce rapid cell death (26).

To fully understand the action of polymyxins on the membrane, molecular dynamics (MD) simulations were employed because they can provide detailed information at the molecular level. For example, coarse-grained MD (CGMD) simulation showed that PmBs aggregate at the sugar headgroup region of OM models composed of lipopolysaccharide (LPS) molecules (27) and restrict LPS

movement but do not spontaneously insert into the membrane. The same group later on reported that the adsorption of PmB also increases the LPS tail order by inducing the formation of crystalline patches in the bilayer (28). They also found that PmBs can spontaneously insert into OM models composed of lipid A molecules and IM models composed of mixtures of phospholipid molecules (27). In contrast, all-atom MD (AAMD) simulations showed that the hydrophobic tail of the PmB only inserts into palmitoyl-oleoyl phosphatidylcholine (POPC) and palmitoyl-oleoyl phospho-L-serine (POPS) bilayers but not the POPC and dimyristoyl phospho-L-serine (DMPS) bilayers where DMPS has saturated dimyristoyl tails (29). Other AAMD simulations revealed that upon binding on OM surfaces, PmBs promote counterion displacement and induce membrane curvature (30).

In this work, we used CGMD simulation to further investigate the mechanism of cationic PmB interacting with both the outer and inner membrane models of bacteria. We systematically analyzed the effects of PmB on the physical properties of membranes, including the lipid packing defect, the orientation order of lipid tails, the membrane bending rigidity, the membrane area, the membrane thickness, the dissociation rate of counterions, and the lipid diffusion coefficient. For comparison, we also studied two other AMPs, melittin (Mel) and protegrin-1 (Pg1), which have typical α -helical and β -turn secondary structures that interact with the IM model. Specifically, we also simulated the adhesion of a vesicle and a planar membrane in the presence or absence of PmB to test the intermembrane contact mechanism. Our results demonstrate that PmB does not penetrate into the IM through traditional mechanisms, such as making holes in the membrane; instead, it acts to compact and stiffen the membrane surface and restrict the movement of lipids. Nevertheless, the binding of PmB does disturb the OM model by displacing the counterions and loosening the packing of LPS. The presence of PmB also promotes intermembrane adhesion and lipid exchange. These findings suggest that PmB may deprive the biological activity of Gram-negative bacteria by sterilizing the cell.

METHODS

Simulation systems

We simulated PmB, Mel, and Pg1 peptides interacting with the inner membrane model, PmBs interacting with the outer membrane model, and the adhesion of a vesicle and a planar bilayer membrane mediated with and without PmB. These simulation systems are summarized in Table 1.

Peptides

The initial atomic coordinates of the PmB were obtained from the NMR measurement (31). The initial structures of melittin (Protein Data Bank, PDB: 2MW6) and protegrin-1 (PDB: 1ZY6) were obtained from the RCSB PDB (<https://www.rcsb.org>). They were then mapped from AA to CG resolution by using the Martini mapping scheme (see Figs. 1 A and

TABLE 1 Simulated Systems

Peptide	Membrane	Lipid Composition	System Setup	Simulation Length
PmB	IM model	symmetric bilayer of mixed POPE/POPG lipids	1352 lipids; 0, 14, 27, 41, 54, 68 PmBs; (P/L: 0, 1, 2, 3, 4, 5%)	1000 ns; three parallel simulations
Mel	IM model	symmetric bilayer of mixed POPE/POPG lipids	1352 lipids; 0, 14, 27, 41, 54, 68 Mels; (P/L: 0, 1, 2, 3, 4, 5%)	1000 ns; three parallel simulations
Pg1	IM model	symmetric bilayer of mixed POPE/POPG lipids	1352 lipids; 0, 14, 27, 41, 54, 68 Pg1s; (P/L: 0, 1, 2, 3, 4, 5%)	1000 ns; three parallel simulations
PmB	OM model	symmetric bilayer of Re LPS	288 Re LPS; 0, 9, 17, 26, 35, 44 PmBs; (P/L: 0, 1, 2, 3, 4, 5%)	3000 ns; three parallel simulations
PmB	vesicle-planar membrane	one vesicle and one planar bilayer of mixed POPE/POPG lipids	1352 lipids in vesicle; 3360 lipids in planar bilayer; 0, 1 PmBs	500 ns; three parallel simulations

S2; (32,33)). Peptide molecules were uniformly placed onto the surface of the previously equilibrated membrane.

Inner membrane model

A symmetric bilayer membrane consisting of 1352 mixed phospholipids (75% phosphatidylethanolamine (POPE) and 25% phosphatidylglycerol (POPG)) was built to mimic the inner membrane of general Gram-negative bacteria. The molecular structure of POPE is shown in Fig. 1 B. The bilayer was immersed in a box with a size of $20 \times 20 \times 12 \text{ nm}^3$. Then, the coarse-grained simulation using the Martini phospholipid force field (34,35) was performed for 1 μs to equilibrate the membrane.

Outer membrane model

The outer membrane of Gram-negative bacteria is an asymmetric bilayer. Its outer leaflet is composed of LPSs and phospholipids, and its inner leaflet is composed of phospholipids (36,37). For simplicity, we used symmetric bilayer containing 288 Re LPS (rough (R)-form LPS isolated and purified from *Escherichia coli*, i.e., lipid A plus two 3-deoxy-D-manno-oct-2-ulosonic acid (KDO) sugars; Fig. 1 C) to mimic the OM following the work of Khalid and co-workers (28) and Soares and co-workers (30). The initial molecular structure of Re LPS was obtained from (38). This level of LPS was deliberately chosen so as to maximize the likelihood of the observed OM disruption by PmB (39,40). The bilayer was also equilibrated for 1 μs before the peptides were added.

Vesicles-planar membrane

A vesicle composed of 1352 lipids was placed on the top of a planar bilayer membrane composing 3360 lipids (POPE/POPG = 3:1). The separation be-

tween the apposed membrane surfaces was $\sim 3.5 \text{ nm}$ to prevent undesired adsorption at the early equilibration stage.

Parameters and protocol

CGMD simulations were performed by using the Martini force field in version 5.0.4 of the GROMACS package (41–44). The CG bead type of the molecules and the force parameters are given in Table S1. The membranes (being void of any peptides) were equilibrated for 1 μs at a unified temperature of 300 K after initial energy minimization. The temperature chosen here is in accord with the previous simulation work by Soares and co-workers (30). Simulations were run in a constant-number, constant-pressure, and constant-temperature ensemble with periodic boundary conditions. The pressure was coupled to 1 bar using a semiisotropic pressure coupling with the Parrinello-Rahman barostat (time constant of 1 ps) (45,46). The temperature was coupled to a Nose-Hoover heat bath (time constant of 1 ps) (47). The neighbor list was updated every 10 steps. After equilibration of the membrane, 14–68 AMP molecules (or 9–44 PmBs for OM model simulations) were uniformly placed $\sim 2 \text{ nm}$ away from one surface of the membrane with peptide/lipid (P/L) molar ratio ranging from 1 to 5%. The OM model was neutralized with Ca^{2+} ions, whereas the IM model was neutralized with Na^+ ions. When the peptides were added to the system, water beads in the same amount of the charges of the peptides were randomly replaced by Cl^- ions. The simulation time of each trajectory was set to 1 μs for the IM-peptide systems and 3 μs for the OM-peptide systems. Three parallel simulations were conducted for each system to collect statistical data.

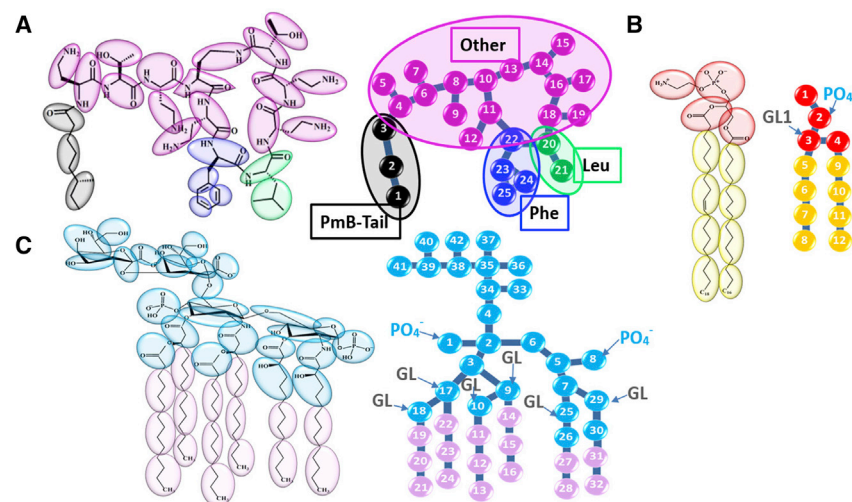


FIGURE 1 Molecular structures of PmB (A), POPE (B), and Re LPS (C) and their corresponding CG mappings. For PmB, the CG charged beads are in magenta; the hydrophobic beads of the fatty acid tail, Phe and Leu are in black, blue, and green, respectively. For POPE, the CG hydrophilic head beads are in red; the hydrophobic tail beads are in yellow. For Re LPS, the hydrophilic head beads are in cyan, and the hydrophobic tail beads are in pink. In (B) and (C), PO_4^- is the phosphate bead, GL is the glycerol bead, and GL1 is the nearest GL bead to PO_4^- . To see this figure in color, go online.

Simulation analyses

To explore the structural, kinetic, and elastic variation of membrane before and after peptide binding, we analyzed the properties of the membrane in terms of the lipid packing defect, the orientation order of lipid tails, the lateral diffusion coefficient of lipids, the membrane bending rigidity, and the dissociation rate of divalent counterions. Up to 1000 samples with a time separation of 500 ps were evenly chosen from one trajectory in the last 500 ns for these calculations.

Lipid packing defect

The adsorption of peptides changes the atomic density profiles and the lateral pressure across the bilayer. However, such analyses are less informative for the interfacial region where peptides are adsorbed. To circumvent this limitation, we used a method of membrane surface analysis provided by Vanni and co-workers (48,49). This method allows for the identification of chemical defects where hydrocarbon chains are accessible to the solvent and geometrical defects where voids are deeper than the glycerol (GL) backbone. The general steps are as follows. The membrane plane was divided into grid lattices at a resolution of 0.1 nm. For each grid cell, we scanned lipid beads in the opposite normal direction of the peptide-bound leaflet and judged their types. If the first encountered bead was a polar head bead, then the grid point was discarded. If an aliphatic bead was encountered, then we retained the grid point and defined it as a chemical defect of size 0.01 nm². If the first bead was aliphatic and its vertical position was below the nearest glycerol (GL1) bead, then the grid point was categorized as a geometrical defect of size 0.01 nm². The geometrical defects represent a subcategory of chemical defects. The scheme of the method used for detecting lipid packing defects is presented in Fig. S1 A. If adjacent elementary defects merged, they resulted in a larger defect.

Orientation order of lipid tails

The adsorption of certain peripheral peptides onto biological membranes also induces mechanical deformations in the geometrical arrangement of the lipids, such as the orientation order of the lipid tails, S_{chain} , which is calculated as follows:

$$S_{\text{chain}} = 0.5 \langle 3 \cos^2 \theta - 1 \rangle. \quad (1)$$

Here, θ is the angle between the normal of the bilayer plane and the orientation along the hydrocarbon chain, which is defined as the vector between the first and last hydrocarbon beads (Fig. S1 B). The ensemble average was over all the lipids in the membrane and the trajectory samples. The values of 1, -0.5, and 0 indicate perfect alignment, antialignment, and random orientation, respectively.

Diffusion coefficient of lipids

In addition to the structures, peptide binding also affects the thermodynamic properties of the membrane, such as the lateral diffusion coefficient (D_A) of the lipids. To evaluate D_A , we first calculated the mean-square displacement of the lipid headgroups or the lipid tail groups along the membrane plane. Then, the D_A of type A particles is determined via the Einstein relation as follows:

$$D_A = \frac{\lim_{t \rightarrow \infty} \langle \|r_i(t) - r_i(0)\|^2 \rangle_{i \in A}}{4t}. \quad (2)$$

This can be obtained by using the *g_msd* command in the GROMACS package (50,51).

Membrane bending rigidity

Another important thermodynamic property of the membrane is the membrane bending rigidity κ , which can be obtained by fitting the spectra of the

longitudinal lipid orientation fluctuations for a bilayer with modest size (52–54). In this method, the bilayer was mapped to a coarser discrete grid with spacing h (~ 1.3 nm in our simulation). In each lattice, the average lipid tail orientation vectors were first projected onto the x - y plane and then mapped onto a two-dimensional real-space grid that yielded a transverse vector $\mathbf{n}^\alpha(\mathbf{r})$ ($\alpha = 1$ and $\alpha = 2$ denote the upper and lower monolayer, respectively). Here, $\mathbf{r} = h\mathbf{m}$, $\mathbf{m} = m_x\mathbf{i} + m_y\mathbf{j}$ with (m_x, m_y) representing the current lattice. The Fourier transformation of the lipid orientation vector $\mathbf{n}(\mathbf{r}) = (1/2)[\mathbf{n}^1(\mathbf{r}) - \mathbf{n}^2(\mathbf{r})]$ is obtained as follows:

$$\hat{\mathbf{n}}_q = \frac{h^2}{L_x L_y} \sum_{\mathbf{m}} \mathbf{n}(\mathbf{r}) e^{-i\mathbf{q} \cdot \mathbf{r}}. \quad (3)$$

Here, $\mathbf{q} = ((2\pi m_x/L_x), (2\pi m_y/L_y))$, where $(-L_x/2h) \leq m_x < (L_x/2h)$ and $(-L_y/2h) \leq m_y < (L_y/2h)$. The thermal fluctuations in the lipid orientation are as follows:

$$S_q = L_x L_y \left\langle \left| \hat{\mathbf{n}}_q \right|^2 \right\rangle = \frac{k_B T}{\kappa q^2}. \quad (4)$$

Here, $\hat{n}_q^\parallel = [\mathbf{q} \cdot \hat{\mathbf{n}}_q]/q$ is the longitudinal component of $\hat{\mathbf{n}}_q$. Fitting of Eq. 4 as a function of q gives the bending rigidity κ . It is worth noting that this method is valid only for a homogeneous flat bilayer. Therefore, we first calculated the κ_s of a membrane with the same number of peptides (i.e., with peptide concentration of 2P/L) symmetrically bound to both leaflets, and then we calculated the κ_0 of a peptide-free membrane. The bending rigidity of the membrane (noted by κ_u) in which only one of its leaflets is bound by peptides (i.e., with peptide concentration of P/L) is thus $\kappa_u = (\kappa_s + \kappa_0)/2$.

Dissociation rate of divalent counterions

The dissociation rate of divalent counterions (Ca^{2+}), α , was computed to identify the binding effect of the peptides onto the OM surface. To estimate α , we first calculated and plotted the density distribution of the Ca^{2+} ion and the PO_4^- group in the direction of the bilayer normal. The distance between the left half peak (proximal to the membrane center) of the PO_4^- group and the right half peak (distal to the membrane center) of Ca^{2+} ion was defined as R . The calcium ions inside a sphere of radius R centered at the PO_4^- group were considered as adsorbed ions. The dissociation rate of the divalent counterion α is defined as follows:

$$\alpha = 1 - \frac{\langle N_{\text{ads}} \rangle}{N_{\text{PO}_4}}. \quad (5)$$

Here, the number of adsorbed ions $\langle N_{\text{ads}} \rangle$ is the ensemble average of 1000 frames obtained in the last 500 ns of the production run, and N_{PO_4} is the number of phosphate groups.

RESULTS

PmBs interacting with the inner membrane model

We first focused on the inner membrane, which was modeled as a symmetric bilayer membrane composed of a mixture of 75% zwitterionic POPE and 25% anionic POPG phospholipids (see Table 1). PmBs with a P/L mole ratio from 1 to 5% were placed ~ 2 nm above the upper leaflet of the bilayer. At all of the peptide concentrations, PmBs were observed to interact with the upper leaflet surface within only a few nanoseconds. The trajectory trace reveals that the charged DAB residues are largely responsible

for the initial binding process, acting as “docking devices” before contacting the membrane. PmBs then regulate their position and orientation to insert their fatty acid tails and hydrophobic residues (Leu and Phe) preferentially into the hydrophobic core of the membrane (Fig. 2 A). These results confirm the previous research, wherein the electrostatic interaction is responsible for the earlier adsorption of PmB onto the membrane in the long range, whereas the hydrophobic interaction plays a major role for their further interactions in the short range (55).

After the interplay between PmBs and the membrane is equilibrated, the PmBs are found only shallowly adsorbed on the surface of the membrane. They neither disturb nor translocate across the membrane. The density distribution of the fatty acid tails and the Leu and Phe residues in the direction of the bilayer normal shows that the hydrophobic residues mainly remain embedded in the amphipathic interface between the lipid headgroups and tails (Fig. 2 A). The insertion becomes slightly deeper when the P/L mole ratio increases from 1 to 5%, but it is still not enough to induce apparent membrane bends or fluctuations. Meanwhile, the density profile of water has negligible change when the concentration of PmB increases (Fig. 2 A). It indicates that the binding of PmB does not promote obvious water permeation. This behavior is quite different from that commonly observed in which many AMPs induce obvious deformation of the membrane (54,56–64). At high peptide concentrations (P/L > 3%), some PmBs associate into micelle-like clusters because of the saturation of electrostatic attraction between the peptides and the membrane (see Fig. S3). This aggregation weakens the tendency of PmBs to insert into the membrane.

Another assessment of the membrane damage caused by PmB insertion is the lipid packing defect. We computed the size distribution probability of the defects before and after PmB insertion (Fig. 3). There are no distinct differences between the pure membrane and the PmB-bound membrane, indicating that the binding of PmB does not create a lipid packing defect. As noted previously by Vanni et al. (48,49), the probability p of finding a defect declines exponentially as the packing defect size of area, A_d , is determined by $p(A_d) = Be^{-kA_d}$, where k is the exponential decay rate. As shown in Fig. 4 A, the fitting decay rate, k , at different PmB concentrations is almost the same.

To further understand the effect of PmB on the IM model quantitatively, we calculated the degree of confusion of phospholipid tails in terms of chain order S_{chain} (Fig. 4 B). Consistent with the lipid packing defect, the orientation of the lipid tails was not significantly disturbed by the presence of PmB. Surprisingly, the binding of more PmBs even increased the order of the lipid tails, implying that the recruitment of PmBs onto the membrane fills up the vacancies between lipids. This result is quite different from that of common AMPs, which tend to decrease the order of the phospholipids (58,65). The binding of PmBs slightly

increases the area per lipid (Fig. 4 C) and decreases the membrane hydrophobic thickness (Fig. 4 D). These are consistent with the previous simulations by Khalid’s group (27).

In addition to the analyses of the structural properties, we also evaluated the thermodynamic properties of the membrane by monitoring lateral lipid diffusion. We focused on the differences in diffusion between the peptide-bound (upper) and peptide-free (lower) leaflets (Fig. 4 E). Only the lipids in the peptide-bound leaflet are slowed down when the concentration of PmB increases, indicating that the binding of the PmBs restricts lipid movement. In contrast, the binding of PmB exerts negligible effects on the diffusion of lipids in the distal leaflet. The different lipid diffusion coefficients imply that the adsorption of PmB does not induce strong coupling between the two leaflets.

The bilayer bending rigidity is another important property that characterizes the elasticity of the membranes and the energy costs associated with large-scale shape deformations in the bilayer. As shown in Figs. 4 F and S4, the value of the bending rigidity increased from $\kappa_0 = 9.4 \times 10^{-20}$ J for a pure lipid bilayer to $\kappa_u = 9.5, 9.7, 10.1,$ and 10.4×10^{-20} J for bilayers in which one, 1, 2, and 3% PmBs were added unsymmetrically; then, it slightly decreased to 10.1×10^{-20} J at P/L = 4%. This behavior indicates that the insertion of PmB fills up the voids among the lipids and results in a more rigid membrane. As mentioned in the Methods, the calculation of rigidity by fitting the spectra of lipid orientation fluctuation is valid for homogeneous and flat bilayer. At peptide concentrations as high as P/L = 4%, the result may not be accurate enough because the clustering of PmBs altered the homogeneity of the membrane.

Comparison of interactions of cyclic polymyxin B, α -helical melittin, and β -sheet protegrin-1 with the inner membrane

The unusual behavior of PmBs interacting with the IM is in marked contrast to other AMPs. Numerous studies have illustrated that cell death is induced by many AMPs via membrane disruption (54,56–64). The membrane-disruptive peptides usually insert into the lipid headgroup region of the membrane, thinning the chain region, which creates the internal membrane tension at low peptide concentration. Upon reaching a critical concentration, the peptides start to form equilibrated pores to release the tension. Several pore models have been suggested, such as the barrel-stave model (56) for trichogin (57,58), the carpet model (59) for magainin (60,61), the toroidal pore model (62) for magainin 2 (63), the buds and invagination model for melittin (54), and the electroporation model for protegrin-1 (64). For the sake of comparison, we also simulated α -helical melittin and β -sheet protegrin-1 interacting with the IM model and analyzed their effects on the structural and thermodynamic properties of the membrane.

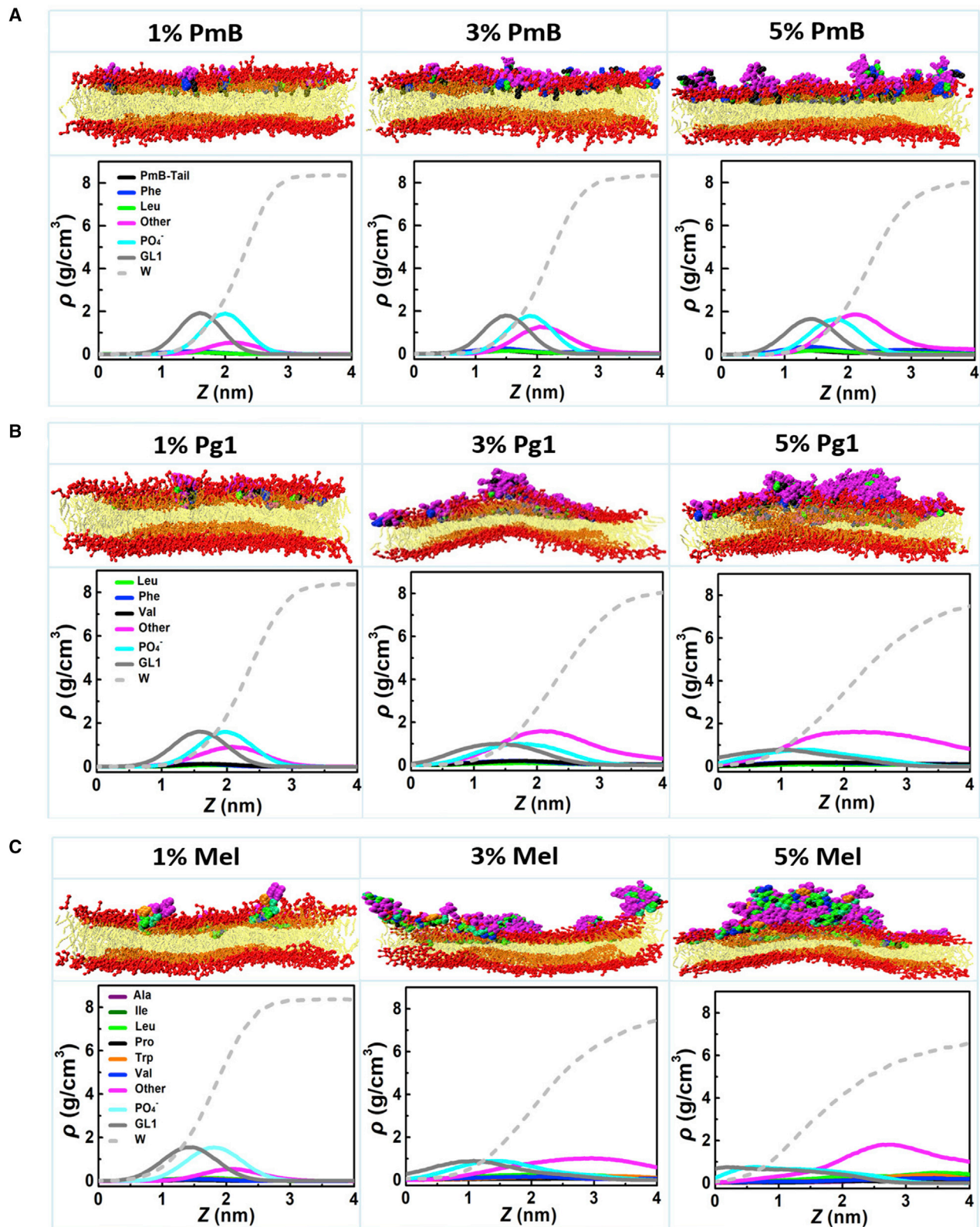


FIGURE 2 Snapshot landscapes of PmB (A), Pg1 (B), and Mel (C) binding to the IM and the corresponding density distribution profiles of the typical functional groups of lipids and residues of peptides along the direction of the bilayer normal (here, “other” refers to the average of the nonhydrophobic residues). To see this figure in color, go online.

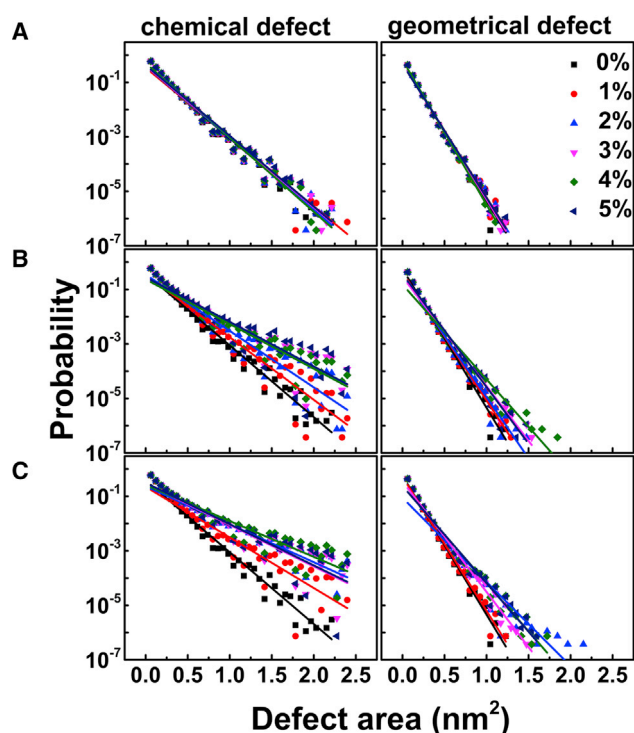


FIGURE 3 Size distribution of the lipid packing defect induced by the binding of PmB (A), Pg1 (B), and Mel (C) to the IM. Solid lines represent the exponential fits at different P/L molar ratios. To see this figure in color, go online.

The binding of Mel and Pg1 significantly bends the membrane as shown in Fig. 2. The broad density distribution of the phosphate (PO_4^-) group and its nearest neighbor glycerol (GL1) group reflects the fluctuation of the membrane. In a consistent way, the differences in lipid packing defect also exhibit the notable dissimilarities between PmB and the other two peptides. The binding of Mel or Pg1 to the bilayer significantly increases the occurrence of large packing defects compared to PmB (Fig. 3). An obvious distribution difference appears when the defect size is larger than 0.5 nm^2 . This size is comparable to a void that can accommodate a hydrophobic residue of Phe or Leu. The large defects, as is more likely induced by Mel and Pg1, indicate that more than one residue of these peptides penetrate into the membrane simultaneously and exclude nearby lipids. By tracking the location of defect of size 1.0 nm^2 on the membrane surface, we indeed found that large defects were directly underneath Mel or Pg1, suggesting that hydrophobic residues, once inserted, stabilize the large packing defects. The exponential decay rate of the defect for these three peptides binding to the IM, as shown in Fig. 4 A, further highlights the specialization of PmB. The k of Mel and Pg1 shows a decreasing trend with increasing peptide concentration, indicating that the insertion of peptide leads to an increased probability of producing large defects. On the other hand, the value of k remains constant at a variety of PmB concentrations, indicating that PmBs only shallowly

adsorb on the surface of the membrane and do not cause extensive damage to the membrane.

Fig. 4 B shows that Mel and Pg1 also cause an enormous disruption in the lipid orientation, especially at increased concentrations. The hydrophobic portions of Mel and Pg1 can insert more deeply into the hydrophobic core of the membrane and significantly disturb the phospholipid tail order. As a consequence, the area per lipid (Fig. 4 C) is significantly increased, whereas the membrane hydrophobic thickness (Fig. 4 D) is decreased.

The restricted lipid movement follows a similar trend for PmB, Mel, and Pg1 (see Fig. 4 E). In this regard, Mel and Pg1 are relatively more efficient than PmB. These results are unsurprising because all of these AMPs are cationic. The electrostatic attraction between these AMPs and the anionic POPG headgroups impedes lipid diffusion.

The changes in bilayer bending rigidity caused by PmB, Mel, and Pg1 are dramatically different (Fig. 4 F). Unlike PmBs, whose binding stiffens the membrane, the binding of Mel and Pg1 softens the membrane by decreasing the bending rigidity. (We noted here that at $\text{P/L} \geq 1\%$, Mel and Pg1 significantly perturbed the flat bilayer structure of the membrane such that the binding rigidity was not available.) This softening effect is a natural consequence of the lower lipid order and larger membrane defects caused by Mel and Pg1. A soft membrane can easily fluctuate and be deformed, which leads to the loss of its protective function. However, rigid membranes fluctuate less and are more stable. This unexpected finding suggests that PmBs can even protect the inner membrane from being damaged.

PmBs interacting with the outer membrane model

To fully understand the action of PmBs on Gram-negative bacteria, we also simulated the binding of PmB to the outer membrane model. Here, we used a bilayer composed of Re LPS (39) to mimic the outer membrane of *E. coli* (see Table 1 and the Methods for a description of the simulation setup). Because one LPS molecule has six tails, threefold that of a phospholipid molecule, for consistency, we define the peptide concentration (still denoted by P/L) as one-third that of the peptide/LPS molar ratio.

Typical snapshots of PmBs binding to the OM model are presented in Figs. 5 and S5. Compared to their interactions with the IM, PmBs tend to aggregate into micelle-like structures on the LPS bilayer surface at low peptide concentrations. Although isolated single PmB molecules have a certain ability to insert their fatty acyl tails and hydrophobic residues into the lipid A tails, the penetration depth is shallow, as indicated by the density profile in Fig. 5. Similar to the case of PmBs binding to the IM model, PmBs also induce negligible fluctuations in the OM model.

Although the shape of the OM is not significantly changed by PmB binding, more PmBs induce larger chemical Re LPS packing defects (Fig. 6) such that the

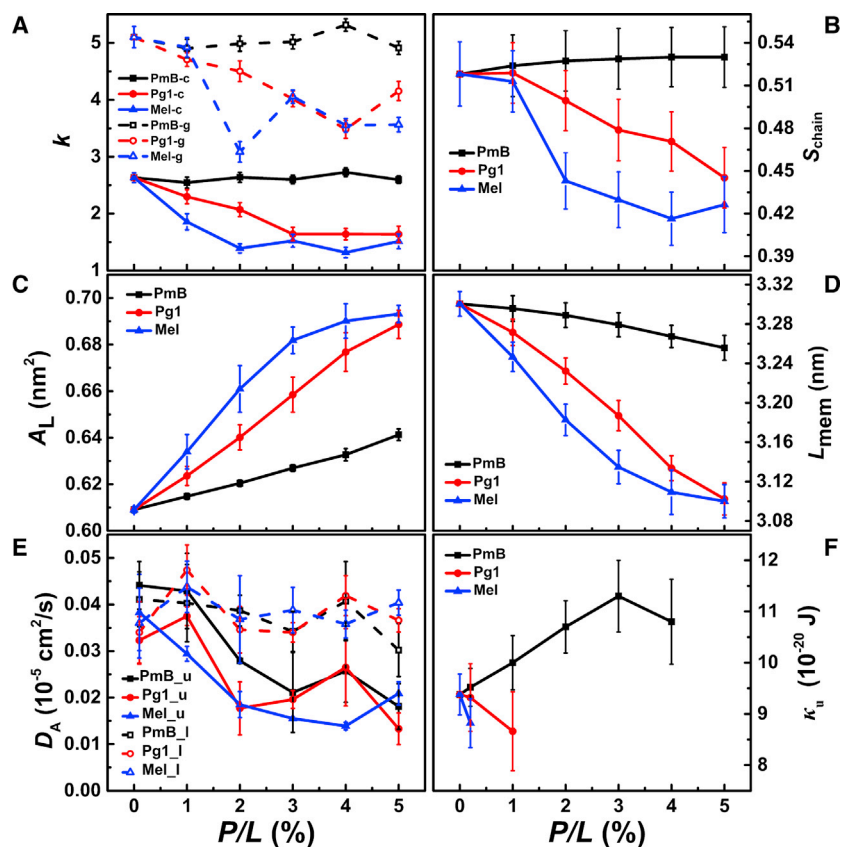


FIGURE 4 Exponential decay rate of chemical (-c) and geometrical (-g) lipid packing defects, k (A); lipid tail order, S_{chain} (B); area per lipid, A_L (C); membrane thickness, L_{mem} (D); lateral lipid diffusion coefficient of upper (-u) and lower (-l) leaflets, D_A (E); and membrane bending rigidity, κ_u (F), induced by the binding of PmB, Pg1, and Mel to the IM model at various peptide concentrations. Statistical errors were obtained from three parallel simulations. To see this figure in color, go online.

exponential decay rate, k , declines when the concentration of PmB increases to as much as $P/L = 2\%$ (Fig. 7 A). This is contrary to the case of the PmB interacting with the IM but similar to that of Mel and Pg1 (Figs. 3 and 4 A). Nevertheless, the binding of PmB does not induce significant geometrical defects, implying that the penetration of PmB is shallow. In addition, the orientation order of the Re LPS tails exhibits declines as the peptide concentration increases (Fig. 7 B). As a consequence, the membranes occupy more area (Fig. 7 C) and become thinner (Fig. 7 D). These results imply that the presence of PmB loosens the Re LPS packing, that is, the PmB binding releases the divalent counterions that are used to link LPS. As shown in Fig. 7 E, the dissociation rate (α) of Ca^{2+} from the peptide-bound leaflet of the OM exhibits a significant shoot-up as the concentration of PmB increases, whereas α of the peptide-free leaflet shows a slight decrease because of the transfer of the ions via periodic boundaries. When $P/L > 2\%$, despite more Ca^{2+} being released, PmBs tend to aggregate and cannot sufficiently penetrate into the membrane, such that the loosening effect becomes relatively weak.

We also monitored the lateral diffusion of Re LPS to characterize the dynamic properties of the membrane. In the absence of PmB, the average lateral diffusion coefficient is $0.0230 \times 10^{-5} \text{ cm}^2/\text{s}$. In the presence of PmB at a concentration of $P/L = 1\%$, the diffusion constants of Re LPS for both the PmB-bound and the PmB-free leaflets decrease to

$0.0075 \times 10^{-5} \text{ cm}^2/\text{s}$ (Fig. 7 F), showing that the LPS movement is restricted by the binding of the PmB. The symmetrical nature of the movement restriction is caused by the binding of counterions released from the PmB-bound leaflet onto the PmB-free leaflet via the periodic boundary conditions in the simulations. At even higher peptide concentrations, the aggregation of PmB weakens the restriction effect.

We did not estimate the bending rigidity of Re LPS by using the method of fitting the spectra of the longitudinal lipid orientation fluctuations because this method is applicable only to phospholipid bilayers with bending rigidity that is mainly determined by lipid tails. For Re LPS, the polysaccharide components also significantly contribute to the bending rigidity. A reliable method could be to fit the spectra of the height fluctuations of the membrane. However, the latter method requires a very large membrane patch, which is out of reach of the capability of current simulation.

PmB triggers robust intermembrane adhesion

The finding that the IM remained intact after PmB treatment motivated us to explore other possible antibacterial actions, such as intermembrane adhesion or fusion. To avoid the limitation of periodic boundary condition, we simulated the contact pathway between a vesicle and a planar bilayer membrane with or without mediated PmB. The detailed

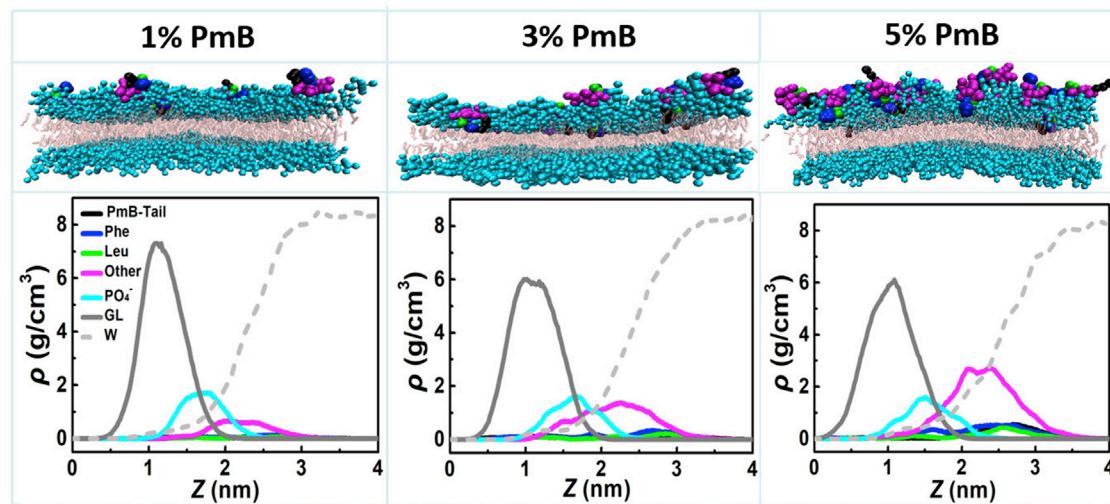


FIGURE 5 Snapshots of the PmBs binding to the OM and the corresponding density distribution profiles of the typical functional groups of the LPS and residues of the peptides along the direction of the bilayer normal. Here, the density of PO_4^- is the average of two PO_4^- groups, and the density of the glycerol bead is the average of six glycerol bead groups of Re LPS as marked in Fig. 1 C. To see this figure in color, go online.

simulation setup with molecular compositions is presented in Table 1 and is explained in the Methods. Three independent parallel simulations were performed.

Fig. 8 shows that when no PmB is presented in between the vesicle and the planar membrane, the kiss contact occurs at 277 ns (or 274 or 225 ns in another two parallel simulations). On the other hand, in the presence of only one

PmB molecule, the initial membrane contact occurs quickly at 17 ns (or 14 or 22 ns). Then, the membranes adhere and exchange lipids. In 500 ns, 136 (or 135 or 138) lipids move from the planar bilayer to the vesicle with the aid of PmB (at a rate of 0.3 lipid/ns), whereas only 46 (or 41 or 55) lipids exchange in the PmB-free system (at a rate of 0.2 lipid/ns). It is noteworthy that the peptide varies its posture in the process of adhesion (Fig. 8 C). At the kiss contact point, the PmB molecule inserts its fatty acyl tail and hydrophobic residues into the vesicle membrane and then rolls over and inserts its fatty acyl tail into the planar membrane. Finally, on the basis of its position, the peptide resembles a double-headed sucker with its two hydrophobic residues gripping the vesicle and its hydrophobic tail gripping the planar membrane, respectively, or vice versa. This bidirectional attraction of the three PmB anchor tails promotes adhesion between the two membranes.

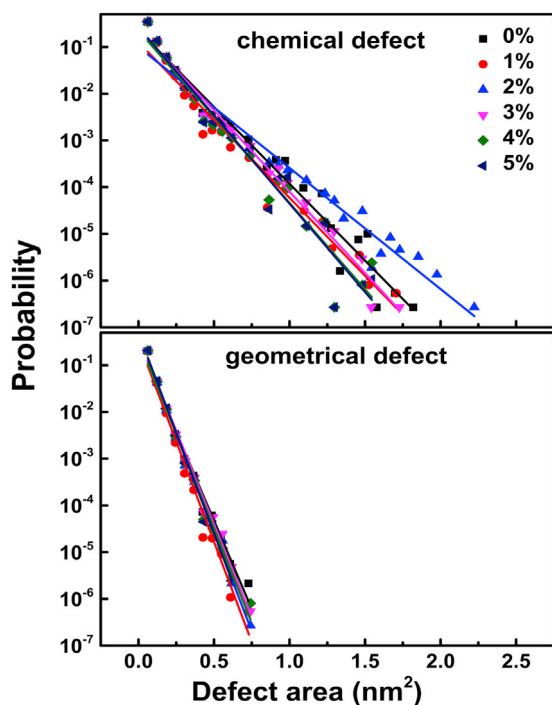


FIGURE 6 Size distribution of lipid packing defects induced by the binding of PmB to the OM. The solid lines are the exponential fits at different P/L molar ratios. To see this figure in color, go online.

DISCUSSION

Polymyxins have successfully been used in the clinic to control the infections of MDR Gram-negative bacteria, affecting the bacteria in a far more complex manner than originally assumed. Our coarse-grained simulations of polymyxin B interacting with both the inner and outer membrane models reveal that the binding of this antimicrobial peptide loosens the LPS packing of the outer membrane but stiffens the inner membrane and promotes cell adhesion. Here, we compare our results with previous experimental and simulation results and discuss the action of PmBs on the bacterial cell.

Our finding of the shallow adsorption of PmB (indicated by the density profiles of the residues and the water penetration) onto the IM is in agreement with the previous work of

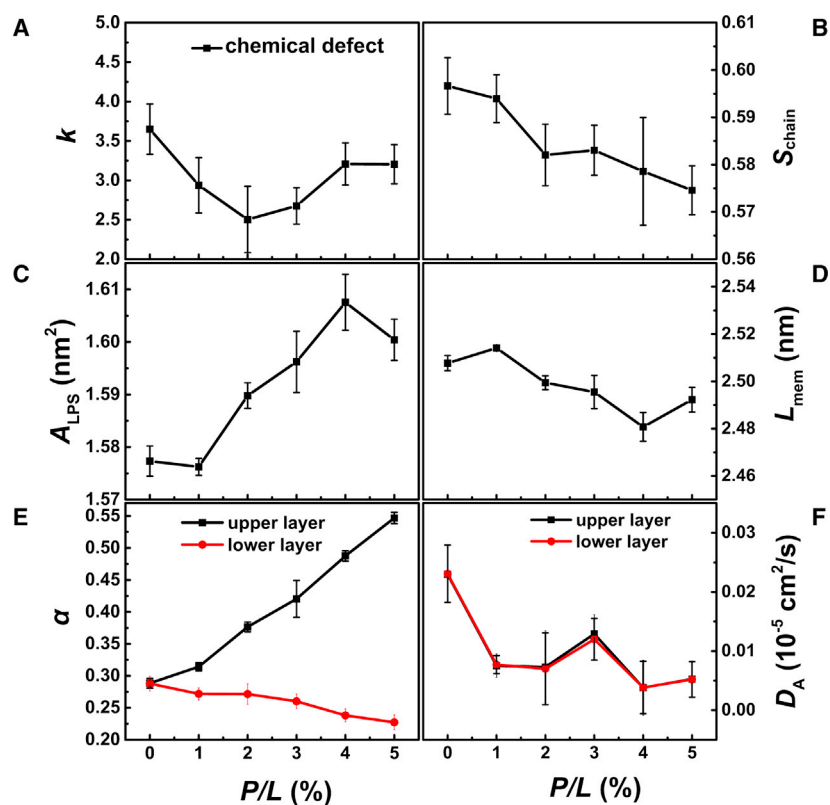


FIGURE 7 Exponential decay rate of lipid packing defect, k (A); orientation order of Re LPS tails, S_{chain} (B); area per LPS, A_{LPS} (C); membrane thickness, L_{mem} (D); dissociation rate of divalent counterion, α (E); and lateral LPS diffusion coefficients, D_A (F), induced by the binding of PmBs to the OM at various peptide concentrations. Statistical errors were obtained from three parallel simulations. To see this figure in color, go online.

Khalid's group (27,28) who also employed CGMD as well as AAMD simulations by using GROMACS software. In addition, our simulations and analyses demonstrated that the binding of PmB to the IM fills up the lipid packing vacancies, which slightly increases the lipid tail order and membrane bending rigidity and restricts lipid diffusion. These properties indicate that PmB adopts a unique bactericidal mechanism by stiffening the IM, which stands in a remarkable contrast to the common mechanism by which

many AMPs kill bacteria by damaging the physical structure of membranes (54,56–64), including Mel and Pg1, which were also simulated herein.

Although numerous experimental studies from the 1990s onward widely accepted that PmBs likely damage the membrane in an undiscovered way to infiltrate the cell and kill it, by 2009, Mortensen et al. (66) suggested another possible mechanism. They used atomic force microscopy to evaluate the changes in *Pseudomonas aeruginosa* morphology and

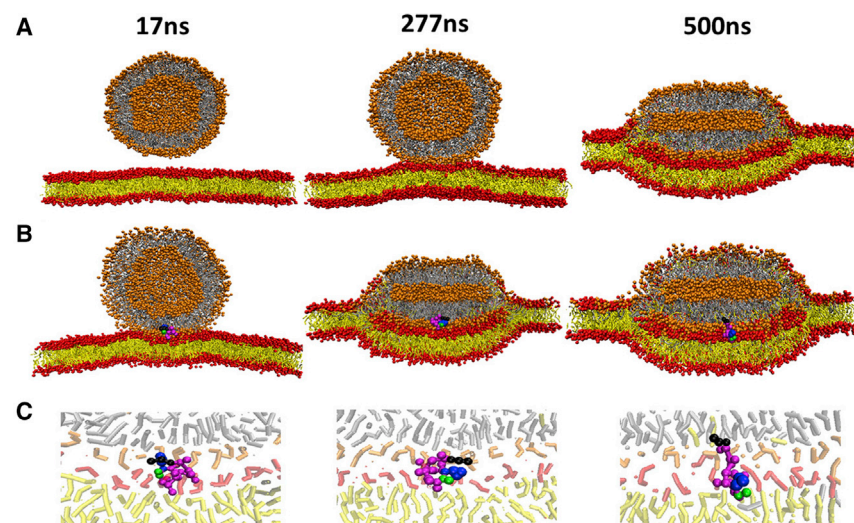


FIGURE 8 Snapshots of the process by which a vesicle and a planar bilayer membrane composed of POPE/POPG lipid adhere without (A) and with (B) PmB mediation. (C) Amplified snapshots of the contact region to illustrate the posture of the PmB are shown. To see this figure in color, go online.

nanomechanical properties after exposure to colistin and found a significant increase in the rigidity of the bacterial cell wall as well as suppressed cell division (66). Subsequently, Soon et al. (67) put forward that colistin softened the colistin-susceptible *Acinetobacter baumannii* cells at low peptide concentrations but significantly increased cellular rigidity at high peptide concentrations (67). They attributed the stiffening effect to the saturation of specific LPS binding sites by colistin, which had the potential to amplify the degree to which the peptides could bind nonspecifically to other components of the OM. Recently, Nagle's group (68) found that colistin produced a softening of model Gram-negative inner membranes at an intermediate P/L molar ratio but stiffening at lower and higher peptide concentrations (68). Our work confirmed the PmB-induced stiffening of the phospholipid's IM at high peptide concentration. According to our simulations, we attribute the membrane stiffening to two possible factors: 1) the neutralization effect induced by multisite charged PmB decreases the electrostatic repulsion between PO_4^- groups, and 2) the specific lipid-like conformation with a ring-sheet head and long fatty acyl chain of PmB permits it to insert into the membrane and fill up the voids between lipids.

It is well known that the membrane-dependent functions of cells, such as protein trafficking and cell signaling, rely heavily on the fluidity of the lipid membrane (69). In contrast, the stiffening of the membrane reduces the cellular biological activity to prevent it from exchanging substances or elongating in a step toward division (66). Based on this knowledge and our results, we propose that PmB might be fatal to the bacteria by sterilizing the cell and not by destroying the local structures of the cell membrane (especially IM). Such specific behaviors of PmBs also make them suitable for clinical use with the least cytotoxicity.

Different actions of PmB on the Re LPS OM model from the IM model were observed in our simulations. Because Re LPS molecules pack more tightly through the linking of both monovalent and divalent counterions, PmBs have a tendency to aggregate on the surface of OM rather than insert into the membrane. Nevertheless, their binding to the OM restricts the motion of Re LPS, in agreement with previous CGMD results (27,28). Reference (28) also claimed that PmBs increased the order within the LPS bilayers by inducing the formation of crystalline patches, but we did not observe any crystalline patches. A possible reason is that PmBs were symmetrically loaded onto two leaflets of the LPS bilayer in (28) but were unsymmetrically loaded onto one leaflet in our simulations.

Previous AAMD simulations showed that PmBs promote the release of Ca^{2+} , enabling them to insert their hydrophobic tails and residues into the outer membrane, thus weakening lipid packing in the LPS leaflet and inducing membrane expansion and curvature (30). Our CG simulation also showed that the adsorption of PmB displaces the Ca^{2+} counterions and perturbs the OM model by decreasing

the orientation order of the LPS tails and creating more lipid packing defects. However, the membrane curvature induced by PmB in our simulation was not obvious, because in our case, the PmBs tend to associate into clusters at peptide concentrations compatible with those in AAMD simulations (30), which inhibits their tendency to insert into the LPS tail region. The Martini model may exaggerate the protein-protein interaction and lead to overestimated aggregation rate (70). Nevertheless, the CG method provides an accessibility to long-scale simulation, and the fault of peptide aggregation is within the range of acceptable level.

The softening of the cell wall was also observed in atomic force microscopy measurements for *A. baumannii* treated with colistin at minimum inhibitory concentration, which showed a reduction in cell rigidity (67). It was proposed that at this concentration, colistin may specifically bind to LPS and destabilize their packing (67). The finding that PmB-induced loosening of the Re LPS membrane in our simulation explains the experimental results well.

In addition to altering the structure and thermodynamic properties of the cell membrane, PmBs may also induce the formation of intermembrane contacts (24,25,71,72). Our simulations showed that PmB can trigger quick membrane adhesion and lipid exchange between a vesicle and a planar bilayer. Even a single PmB molecule could accelerate the contact speed by as much as one order of magnitude. The significant robust adhesion induced by PmB is explained by two possible mechanisms: 1) the multisite positive charges of PmB attract anionic lipids in two adjacent membranes, and 2) the PmB fatty acyl tail and two hydrophobic residues bidirectionally insert into the opposed membranes and pull them together until they adhere. The periplasmic space of Gram-negative bacteria is only $\sim 12\text{--}15$ nm; thus, permeated PmBs across the OM may induce adhesion between the inner and outer membranes.

CONCLUSIONS

The longstanding and unexplained puzzle of the antibacterial mechanism of polymyxin B on Gram-negative bacteria was studied by MD simulations at CG resolution. Our study shows that PmBs bind onto the Re LPS outer membrane mainly in micelle-like clusters. They displace the counterions and subsequently decrease the orientation order of the LPS tails and create greater lipid packing defects, which may allow PmBs to pass through the OM via a self-promoted uptake pathway. Upon binding to an inner membrane composed of mixed POPE/POPG lipids, PmBs are shallowly adsorbed onto the membrane surface with their fatty acyl tails and its hydrophobic residues inserting into the lipid tail region. Rather than damaging the membrane structure in the manner of many other antimicrobial peptides, the insertion of PmBs fills up the lipid packing defect and increases the lipid tail order and eventually stiffens the

membrane and restricts lipid diffusion. PmBs also mediate intermembrane contact and adhesion. These combined effects cause Gram-negative bacteria to lose their biological activities without harming nearby mammalian cells. The unprecedented mechanisms found here may contribute to paving the way for the development of therapeutic agents targeting bacteria.

SUPPORTING MATERIAL

Supporting Material can be found online at <https://doi.org/10.1016/j.bpj.2019.11.008>.

AUTHOR CONTRIBUTIONS

L.G. and W.F. designed the research. L.F., M.W., and S.Z. performed the research. L.F. and L.G. analyzed data and wrote the article.

ACKNOWLEDGMENTS

This work is supported by the National Natural Science Foundation of China (grant nos. 21673021, 21421003).

REFERENCES

- Evans, M. E., D. J. Feola, and R. P. Rapp. 1999. Polymyxin B sulfate and colistin: old antibiotics for emerging multiresistant gram-negative bacteria. *Ann. Pharmacother.* 33:960–967.
- Li, J., and R. L. Nation. 2006. Old polymyxins are back: is resistance close? *Clin. Infect. Dis.* 43:663–664.
- Li, J., R. L. Nation, ..., K. Coulthard. 2005. Evaluation of colistin as an agent against multi-resistant Gram-negative bacteria. *Int. J. Antimicrob. Agents.* 25:11–25.
- Li, J., R. L. Nation, ..., C. Franklin. 2007. Antibiograms of multidrug-resistant clinical *Acinetobacter baumannii*: promising therapeutic options for treatment of infection with colistin-resistant strains. *Clin. Infect. Dis.* 45:594–598.
- Li, J., R. L. Nation, ..., D. L. Paterson. 2006. Colistin: the re-emerging antibiotic for multidrug-resistant Gram-negative bacterial infections. *Lancet Infect. Dis.* 6:589–601.
- Velkov, T., P. E. Thompson, ..., J. Li. 2010. Structure–activity relationships of polymyxin antibiotics. *J. Med. Chem.* 53:1898–1916.
- Kimura, Y., H. Matsunaga, and M. Vaara. 1992. Polymyxin B octapeptide and polymyxin B heptapeptide are potent outer membrane permeability-increasing agents. *J. Antibiot. (Tokyo).* 45:742–749.
- Storm, D. R., K. S. Rosenthal, and P. E. Swanson. 1977. Polymyxin and related peptide antibiotics. *Annu. Rev. Biochem.* 46:723–763.
- Rosenthal, K. S., and D. R. Storm. 1977. Disruption of the *Escherichia coli* outer membrane permeability barrier by immobilized polymyxin B. *J. Antibiot. (Tokyo).* 30:1087–1092.
- Liu, Y. Y., Y. Wang, ..., J. Shen. 2016. Emergence of plasmid-mediated colistin resistance mechanism MCR-1 in animals and human beings in China: a microbiological and molecular biological study. *Lancet Infect. Dis.* 16:161–168.
- Roberts, K. D., M. A. Azad, ..., J. Li. 2015. Antimicrobial activity and toxicity of the major lipopeptide components of polymyxin B and colistin: last-line antibiotics against multidrug-resistant gram-negative bacteria. *ACS Infect. Dis.* 1:568–575.
- Gallardo-Godoy, A., C. Muldoon, ..., M. A. Cooper. 2016. Activity and predicted nephrotoxicity of synthetic antibiotics based on polymyxin B. *J. Med. Chem.* 59:1068–1077.
- Minrovic, B. M., V. B. Hubble, ..., C. Melander. 2019. Second-generation tryptamine derivatives potentially sensitize colistin resistant bacteria to colistin. *ACS Med. Chem. Lett.* 10:828–833.
- Minrovic, B. M., D. Jung, ..., C. Melander. 2018. New class of adjuvants enables lower dosing of colistin against *Acinetobacter baumannii*. *ACS Infect. Dis.* 4:1368–1376.
- Cui, A. L., X. X. Hu, ..., Z. R. Li. 2018. Synthesis and bioactivity investigation of the individual components of cyclic lipopeptide antibiotics. *J. Med. Chem.* 61:1845–1857.
- Koike, M., K. Iida, and T. Matsuo. 1969. Electron microscopic studies on mode of action of polymyxin. *J. Bacteriol.* 97:448–452.
- Zhang, L., P. Dhillon, ..., R. E. Hancock. 2000. Interactions of bacterial cationic peptide antibiotics with outer and cytoplasmic membranes of *Pseudomonas aeruginosa*. *Antimicrob. Agents Chemother.* 44:3317–3321.
- Hancock, R. E. 1984. Alterations in outer membrane permeability. *Annu. Rev. Microbiol.* 38:237–264.
- Hancock, R. E., V. J. Raffle, and T. I. Nicas. 1981. Involvement of the outer membrane in gentamicin and streptomycin uptake and killing in *Pseudomonas aeruginosa*. *Antimicrob. Agents Chemother.* 19:777–785.
- Hancock, R. E., and D. S. Chapple. 1999. Peptide antibiotics. *Antimicrob. Agents Chemother.* 43:1317–1323.
- Hancock, R. E. 1997. Peptide antibiotics. *Lancet.* 349:418–422.
- Hancock, R. E., T. Falla, and M. Brown. 1995. Cationic bactericidal peptides. *Adv. Microb. Physiol.* 37:135–175.
- Clausell, A., M. Garcia-Subirats, ..., Y. Cajal. 2007. Gram-negative outer and inner membrane models: insertion of cyclic cationic lipopeptides. *J. Phys. Chem. B.* 111:551–563.
- Cajal, Y., J. Rogers, ..., M. K. Jain. 1996. Intermembrane molecular contacts by polymyxin B mediate exchange of phospholipids. *Biochemistry.* 35:299–308.
- Cajal, Y., J. Ghanta, ..., M. K. Jain. 1996. Specificity for the exchange of phospholipids through polymyxin B mediated intermembrane molecular contacts. *Biochemistry.* 35:5684–5695.
- Kohanski, M. A., D. J. Dwyer, ..., J. J. Collins. 2007. A common mechanism of cellular death induced by bactericidal antibiotics. *Cell.* 130:797–810.
- Berglund, N. A., T. J. Piggot, ..., S. Khalid. 2015. Interaction of the antimicrobial peptide polymyxin B1 with both membranes of *E. coli*: a molecular dynamics study. *PLoS Comput. Biol.* 11:e1004180.
- Jefferies, D., P. C. Hsu, and S. Khalid. 2017. Through the lipopolysaccharide glass: a potent antimicrobial peptide induces phase changes in membranes. *Biochemistry.* 56:1672–1679.
- Khondker, A., A. K. Dhaliwal, ..., M. C. Rheinstädter. 2019. Membrane charge and lipid packing determine polymyxin-induced membrane damage. *Commun Biol.* 2:67.
- Santos, D. E. S., L. Pol-Fachin, ..., T. A. Soares. 2017. Polymyxin binding to the bacterial outer membrane reveals cation displacement and increasing membrane curvature in susceptible but not in resistant lipopolysaccharide chemotypes. *J. Chem. Inf. Model.* 57:2181–2193.
- Pristovsek, P., and J. Kidric. 1999. Solution structure of polymyxins B and E and effect of binding to lipopolysaccharide: an NMR and molecular modeling study. *J. Med. Chem.* 42:4604–4613.
- de Jong, D. H., G. Singh, ..., S. J. Marrink. 2013. Improved parameters for the Martini coarse-grained protein force field. *J. Chem. Theory Comput.* 9:687–697.
- Monticelli, L., S. K. Kandasamy, ..., S. J. Marrink. 2008. The MARTINI coarse-grained force field: extension to proteins. *J. Chem. Theory Comput.* 4:819–834.
- Marrink, S. J., A. H. de Vries, and A. E. Mark. 2004. Coarse grained model for semiquantitative lipid simulations. *J. Phys. Chem. B.* 108:750–760.

35. Dahlberg, M., and A. Maliniak. 2010. Mechanical properties of coarse-grained bilayers formed by cardiolipin and zwitterionic lipids. *J. Chem. Theory Comput.* 6:1638–1649.
36. Costerton, J. W., J. M. Ingram, and K. J. Cheng. 1974. Structure and function of the cell envelope of gram-negative bacteria. *Bacteriol. Rev.* 38:87–110.
37. Lugtenberg, B., and L. Van Alphen. 1983. Molecular architecture and functioning of the outer membrane of *Escherichia coli* and other gram-negative bacteria. *Biochim. Biophys. Acta.* 737:51–115.
38. Hsu, P. C., D. Jefferies, and S. Khalid. 2016. Molecular dynamics simulations predict the pathways via which pristine fullerenes penetrate bacterial membranes. *J. Phys. Chem. B.* 120:11170–11179.
39. Raetz, C. R. 1990. Biochemistry of endotoxins. *Annu. Rev. Biochem.* 59:129–170.
40. Raetz, C. R., and C. Whitfield. 2002. Lipopolysaccharide endotoxins. *Annu. Rev. Biochem.* 71:635–700.
41. Lindahl, E., B. Hess, and D. van der Spoel. 2001. GROMACS 3.0: a package for molecular simulation and trajectory analysis. *J. Mol. Model.* 7:306–317.
42. Van Der Spoel, D., E. Lindahl, ..., H. J. Berendsen. 2005. GROMACS: fast, flexible, and free. *J. Comput. Chem.* 26:1701–1718.
43. Hess, B., C. Kutzner, ..., E. Lindahl. 2008. GROMACS 4: algorithms for highly efficient, load-balanced, and scalable molecular simulation. *J. Chem. Theory Comput.* 4:435–447.
44. Pronk, S., S. Páll, ..., E. Lindahl. 2013. GROMACS 4.5: a high-throughput and highly parallel open source molecular simulation toolkit. *Bioinformatics.* 29:845–854.
45. Parrinello, M., and A. Rahman. 1981. Polymorphic transitions in single crystals: a new molecular dynamics method. *J. Appl. Phys.* 52:7182–7190.
46. Nosé, S., and M. L. Klein. 1983. Constant pressure molecular dynamics for molecular systems. *Mol. Phys.* 50:1055–1076.
47. Evans, D. J., and B. L. Holian. 1985. The Nose-Hoover thermostat. *J. Chem. Phys.* 83:4069–4074.
48. Vanni, S., L. Vamparys, ..., B. Antony. 2013. Amphipathic lipid packing sensor motifs: probing bilayer defects with hydrophobic residues. *Biophys. J.* 104:575–584.
49. Vamparys, L., R. Gautier, ..., P. F. Fuchs. 2013. Conical lipids in flat bilayers induce packing defects similar to that induced by positive curvature. *Biophys. J.* 104:585–593.
50. Piggot, T. J., D. A. Holdbrook, and S. Khalid. 2011. Electroporation of the *E. coli* and *S. Aureus* membranes: molecular dynamics simulations of complex bacterial membranes. *J. Phys. Chem. B.* 115:13381–13388.
51. Koldsø, H., D. Shorthouse, ..., M. S. Sansom. 2014. Lipid clustering correlates with membrane curvature as revealed by molecular simulations of complex lipid bilayers. *PLoS Comput. Biol.* 10:e1003911.
52. Watson, M. C., E. G. Brandt, ..., F. L. Brown. 2012. Determining biomembrane bending rigidities from simulations of modest size. *Phys. Rev. Lett.* 109:028102.
53. Levine, Z. A., R. M. Venable, ..., F. L. Brown. 2014. Determination of biomembrane bending moduli in fully atomistic simulations. *J. Am. Chem. Soc.* 136:13582–13585.
54. Shi, Y., M. Wan, ..., W. Fang. 2018. Peptide-lipid interaction sites affect vesicles' responses to antimicrobial peptides. *Biophys. J.* 115:1518–1529.
55. Vesentini, S., M. Soncini, ..., A. Redaelli. 2006. Multi-scale analysis of the toraymyxin adsorption cartridge. Part I: molecular interaction of polymyxin B with endotoxins. *Int. J. Artif. Organs.* 29:239–250.
56. Ehrenstein, G., and H. Lecar. 1977. Electrically gated ionic channels in lipid bilayers. *Q. Rev. Biophys.* 10:1–34.
57. Yang, L., T. M. Weiss, ..., H. W. Huang. 2000. Crystallization of antimicrobial pores in membranes: magainin and protegrin. *Biophys. J.* 79:2002–2009.
58. Bobone, S., Y. Gerelli, ..., L. Stella. 2013. Membrane thickness and the mechanism of action of the short peptide trichogin GA IV. *Biochim. Biophys. Acta.* 1828:1013–1024.
59. Pouny, Y., D. Rapaport, ..., Y. Shai. 1992. Interaction of antimicrobial dermaseptin and its fluorescently labeled analogues with phospholipid membranes. *Biochemistry.* 31:12416–12423.
60. Bechinger, B., M. Zasloff, and S. J. Opella. 1993. Structure and orientation of the antibiotic peptide magainin in membranes by solid-state nuclear magnetic resonance spectroscopy. *Protein Sci.* 2:2077–2084.
61. Matsuzaki, K., O. Murase, ..., K. Miyajima. 1994. Orientational and aggregational states of magainin 2 in phospholipid bilayers. *Biochemistry.* 33:3342–3349.
62. Yoneyama, F., Y. Imura, ..., K. Sonomoto. 2009. Peptide-lipid huge toroidal pore, a new antimicrobial mechanism mediated by a lactococcal bacteriocin, lacticin Q. *Antimicrob. Agents Chemother.* 53:3211–3217.
63. Matsuzaki, K., O. Murase, ..., K. Miyajima. 1996. An antimicrobial peptide, magainin 2, induced rapid flip-flop of phospholipids coupled with pore formation and peptide translocation. *Biochemistry.* 35:11361–11368.
64. Lai, P. K., and Y. N. Kaznessis. 2018. Insights into membrane translocation of protegrin antimicrobial peptides by multistep molecular dynamics simulations. *ACS Omega.* 3:6056–6065.
65. Bechinger, B., M. Zasloff, and S. J. Opella. 1992. Structure and interactions of magainin antibiotic peptides in lipid bilayers: a solid-state nuclear magnetic resonance investigation. *Biophys. J.* 62:12–14.
66. Mortensen, N. P., J. D. Fowlkes, ..., M. J. Doktycz. 2009. Effects of colistin on surface ultrastructure and nanomechanics of *Pseudomonas aeruginosa* cells. *Langmuir.* 25:3728–3733.
67. Soon, R. L., R. L. Nation, ..., I. Larson. 2011. Effect of colistin exposure and growth phase on the surface properties of live *Acinetobacter baumannii* cells examined by atomic force microscopy. *Int. J. Antimicrob. Agents.* 38:493–501.
68. Dupuy, F. G., I. Pagano, ..., S. Tristram-Nagle. 2018. Selective interaction of colistin with lipid model membranes. *Biophys. J.* 114:919–928.
69. Berg, J. M., J. L. Tymoczko, ..., L. Stryer. 2015. *Biochemistry*. W. H. Freeman, New York.
70. Javanainen, M., H. Martinez-Seara, and I. Vattulainen. 2017. Excessive aggregation of membrane proteins in the Martini model. *PLoS One.* 12:e0187936.
71. Cajal, Y., O. G. Berg, and M. K. Jain. 1995. Direct vesicle-vesicle exchange of phospholipids mediated by polymyxin B. *Biochem. Biophys. Res. Commun.* 210:746–752.
72. Clausell, A., M. A. Busquets, ..., Y. Cajal. 2004. Polymyxin B-lipid interactions in Langmuir-Blodgett monolayers of *Escherichia coli* lipids: a thermodynamic and atomic force microscopy study. *Biopolymers.* 75:480–490.

Biophysical Journal, Volume 118

Supplemental Information

Polymyxin B Loosens Lipopolysaccharide Bilayer but Stiffens Phospholipid Bilayer

Lei Fu, Mingwei Wan, Shan Zhang, Lianghai Gao, and Weihai Fang

Supplementary Information for

Polymyxin B Loosens Lipopolysaccharide Bilayer but Stiffens Phospholipid Bilayer

Lei Fu, Mingwei Wan, Shan Zhang, Lianghai Gao*, and Weihai Fang

Key Laboratory of Theoretical and Computational Photochemistry, Ministry of Education, College of Chemistry, Beijing Normal University, 19 Xin-Jie-Kou-Wai Street, Beijing 100875, China

Corresponding Author: Lianghai Gao

Email: lhgao@bnu.edu.cn

This PDF file includes:

Table S1

Figure S1 to S5

Table S1. CG beads types and bond parameters of polymyxin B, POPE and Re LPS.

i	type	residue	bond	Length (nm)	K_{bond} (KJ nm ⁻² mol ⁻¹)	angle	θ (degree)	K_{angle} (KJmol ⁻¹)
polymyxin B								
1	C1	AMO	1-2	0.367	5000	1-2-3	177.1	25
2	C1	AMO	2-3	0.362	5000	2-3-4	147.3	25
3	Na	AMO	3-4	0.305	5000	3-4-6	154.7	25
4	P5	DAB	4-5	0.321	5000	4-6-8	156.1	25
5	Qd	DAB	4-6	0.342	200	6-8-10	69.9	25
6	P5	THR	6-8	0.351	200	8-10-13	80.4	25
7	P1	THR	8-9	0.338	5000	10-13-14	134.9	25
8	P5	DAB	8-10	0.318	200	13-14-16	115.0	25
9	Qd	DAB	10-13	0.311	5000	14-16-18	108.4	25
10	P5	DABN	10-11	0.387	200	16-18-20	135.7	25
11	P5	DAB	11-12	0.348	5000	18-20-22	107.6	25
12	Qd	DAB	11-22	0.302	200	20-22-11	122.5	25
13	P1	DABN	22-23	0.332	7500	22-11-10	119.5	25
14	P5	THR	12-20	0.358	200	11-10-8	155.0	25
15	P1	THR	20-21	0.298	7500	11-10-13	98.4	25
16	P5	DAB	20-18	0.326	200	5-4-3	100.2	25

17	Qd	DAB	18-19	0.326	5000	5-4-6	102.9	25
18	P5	DAB	18-16	0.338	200	7-6-4	79.2	25
19	Qd	DAB	16-17	0.329	5000	7-6-8	102.3	25
20	P5	LEU	16-14	0.370	200	9-8-6	105.8	25
21	C1	LEU	14-13	0.305	5000	9-8-10	150.3	25
22	P5	DPHE	6-7	0.291	constraint	12-11-10	74.8	25
23	SC4	DPHE	14-15	0.231	constraint	12-11-22	162.6	25
24	SC4	DPHE	23-24	0.243	constraint	23-22-11	109.9	25
25	SC4	DPHE	23-25	0.289	constraint	23-22-20	121.4	25
			24-25	0.221	constraint	21-20-22	91.6	25
						21-20-18	139.6	25
						19-18-20	92.9	25
						19-18-16	124.0	25
						17-16-18	123.8	25
						17-16-14	112.3	25
						15-14-16	97.6	25
						15-14-13	126.6	25
						22-23-24	99.9	50
						22-23-25	133.3	50
						22-24-25-23	0	50

POPE

1	Qd	NH3	1-2	0.470	1250	2-3-4	120.0	25
2	Qa	PO4	2-3	0.470	1250	2-3-5	180.0	25
3	Na	GL1	3-4	0.370	1250	3-5-6	180.0	25
4	Na	GL2	3-5	0.470	1250	5-6-7	120.0	45
5	C1	C1A	5-6	0.470	1250	6-7-8	180.0	25
6	C3	D2A	6-7	0.470	1250	4-9-10	180.0	25
7	C1	C3A	7-8	0.470	1250	9-10-11	180.0	25
8	C1	C4A	4-9	0.470	1250	10-11-12	180.0	25
9	C1	C1B	9-10	0.470	1250			
10	C1	C2B	10-11	0.470	1250			
11	C1	C3B	11-12	0.470	1250			
12	C1	C4B						

Re LPS

1	Qa	PO1	1-2	0.417	5074	1-2-3	89.5	8
2	P2	GM1	2-4	0.213	21824	1-2-4	82.7	12
3	Nda	GM2	2-6	0.418	5448	1-2-6	158.9	10
4	P1	GM3	3-9	0.320	6057	2-3-9	126.1	8
5	P2	GM4	3-17	0.339	5275	2-3-17	129.6	11
6	P1	GM5	5-8	0.398	7231	2-4-33	137.1	10
7	Nda	GM6	6-5	0.211	17769	2-6-5	151.0	10
8	Qa	PO2	7-25	0.289	5308	3-2-4	162.0	10
9	Na	GL1	7-29	0.296	7684	3-2-6	95.3	11
10	Na	GL2	9-10	0.312	1359	3-9-10	109.8	10
11	C1	C1A	9-14	0.448	1732	3-9-14	118.0	11
12	C1	C2A	10-11	0.400	1613	3-17-18	119.1	10

13	C1	C3A	11-12	0.468	1830	3-17-22	142.0	12
14	C1	C1B	12-13	0.460	1618	4-2-6	96.4	10
15	C1	C2B	14-15	0.468	1820	4-34-33	81.1	15
16	C1	C3B	15-16	0.409	2215	4-34-35	111.1	10
17	Na	GL3	17-18	0.342	1155	5-7-25	110.1	11
18	Na	GL4	17-22	0.437	1274	5-7-29	142.5	23
19	C1	C1C	18-19	0.398	1589	6-5-7	143.6	11
20	C1	C2C	19-20	0.353	3151	6-5-8	101.7	10
21	C1	C3C	20-21	0.408	2193	7-5-8	94.6	10
22	C1	C1D	22-23	0.465	1638	7-25-26	129.4	9
23	C1	C2D	23-24	0.408	2199	7-29-30	136.3	12
24	C1	C3D	25-26	0.305	4607	9-3-17	101.0	11
25	Na	GL5	26-27	0.463	2041	9-14-15	150.9	11
26	Nda	GL6	27-28	0.516	1210	9-10-11	150.9	10
27	C1	C1E	29-30	0.293	3803	10-11-12	150.1	11
28	C1	C2E	30-31	0.464	1848	10-9-14	66.5	11
29	Na	GL7	31-32	0.516	1205	11-12-13	152.4	9
30	Nda	GL8	4-34	0.336	14595	14-15-16	154.1	9
31	C1	C1F	35-36	0.157	13867	17-18-19	145.2	10
32	C1	C2F	35-37	0.347	3108	17-22-23	155.5	9
33	Qa	S01	35-38	0.397	14156	18-17-22	67.8	11
34	SC1	S02	39-40	0.157	24430	18-19-20	149.8	11
35	P2	S03	39-41	0.357	2563	19-20-21	154.5	9
36	SN0	S04	2-3	0.190	constraint	22-23-24	152.3	11
37	P4	S05	5-7	0.197	constraint	25-7-29	104.7	11
38	SC1	S06	33-34	0.224	constraint	25-26-27	142.0	11
39	P2	S07	34-35	0.165	constraint	26-27-28	154.7	9
40	SN0	S08	38-39	0.165	constraint	29-30-31	125.9	10
41	P4	S09	38-42	0.222	constraint	30-31-32	153.9	11
42	Qa	S10				33-34-35	145.5	8
						34-35-36	131.9	9
						34-35-37	118.4	11
						34-35-38	106.4	10
						35-38-42	77.1	12
						36-35-38	86.9	11
						37-35-38	132.6	11
						38-39-40	129.8	11
						38-39-41	118.9	12
						40-39-41	69.5	10

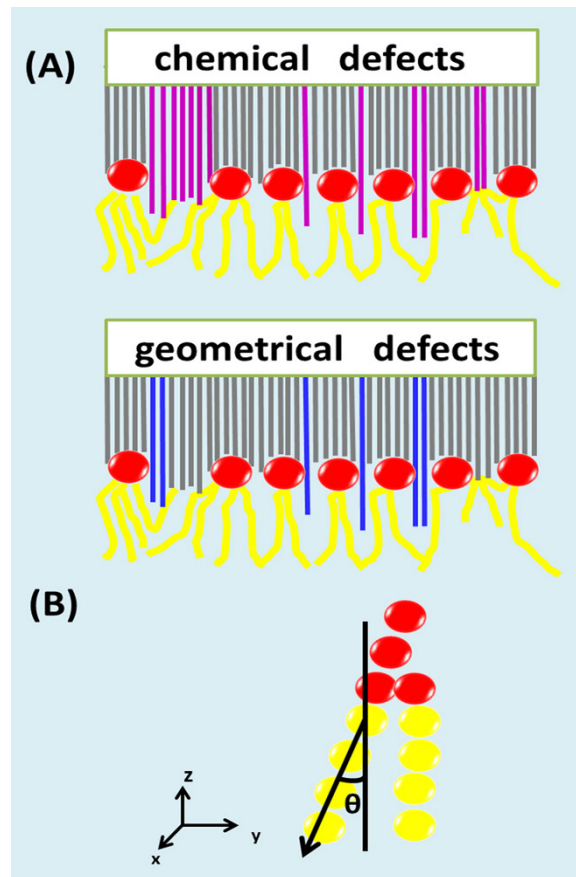


Figure S1. Schematic illustrations of the method for detecting lipid packing defects (A) and the definition of the lipid tail tilt angle (B). The planar bilayer normal is in the z direction. In (A), the chemical defects are represented by magenta lines, geometrical defects are represented by blue lines, and the gray lines are not defects.

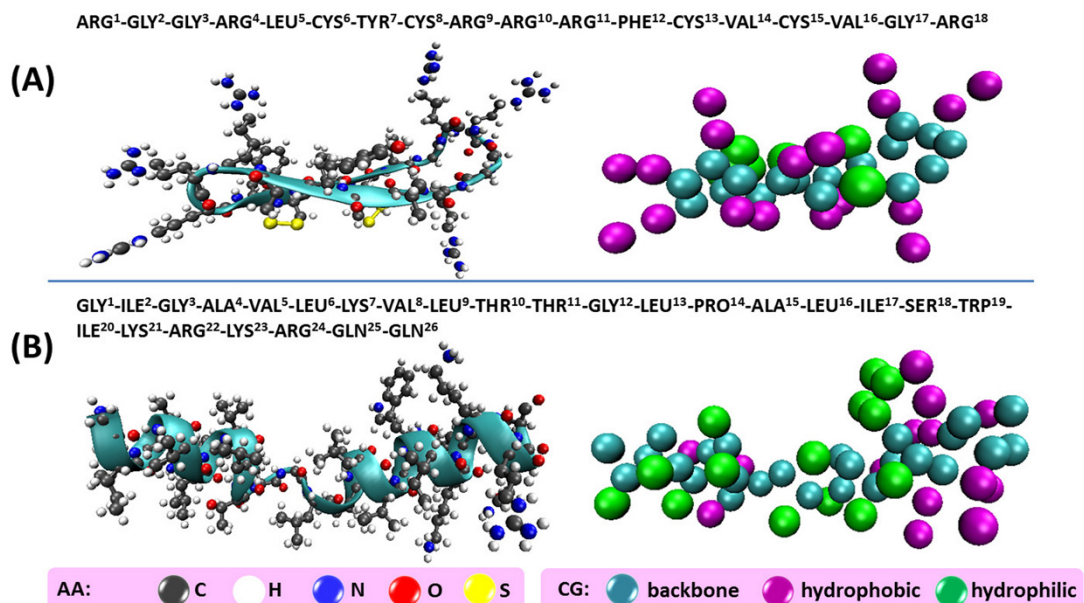


Figure S2. Molecular structures of protegrin-1 (A) and melittin (B) and their corresponding coarse-grained mappings.

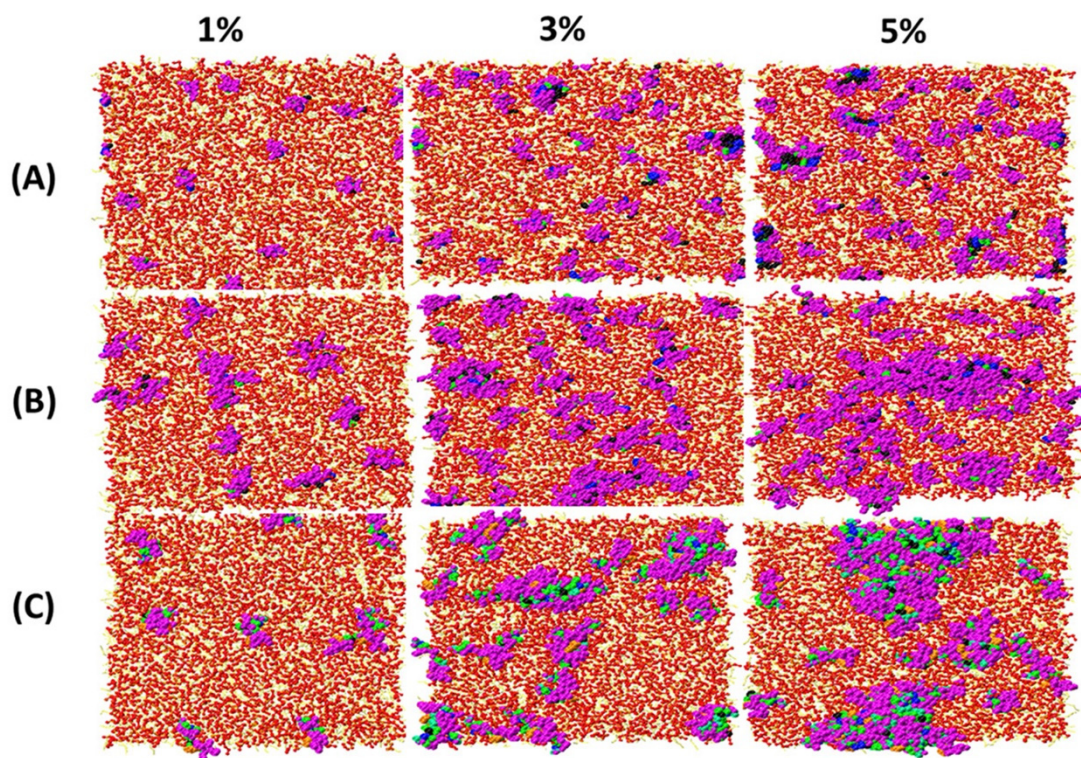


Figure S3. Top view of the snapshots of PmB (A), Pg1 (B) and Mel (C) binding to the inner membrane model.

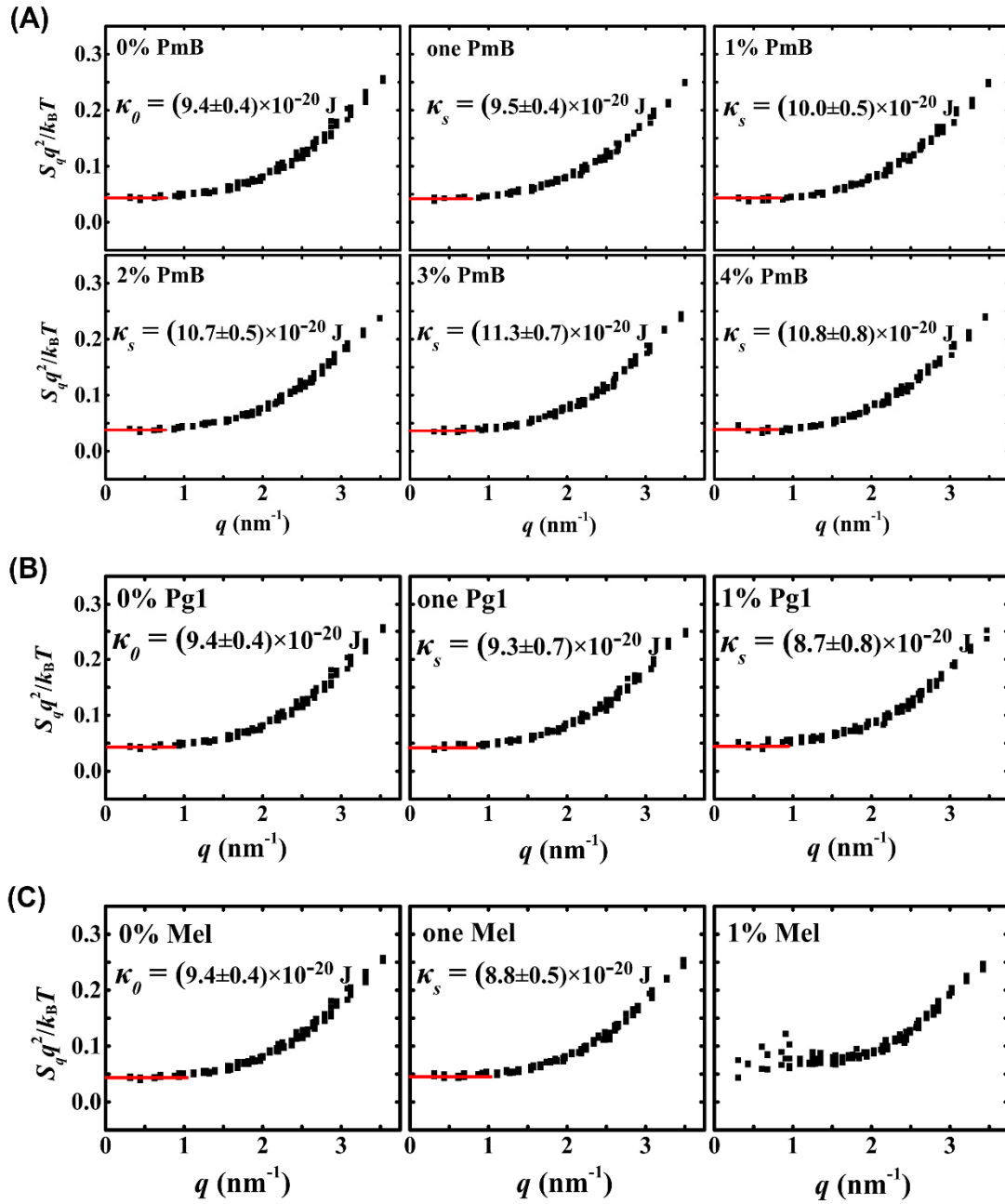


Figure S4. Spectra of the longitudinal lipid orientation fluctuations before and after PmB (A), Pg1 (B) and Mel (B) binding to the membrane. The converged κ_θ and κ_s values were obtained from the plateau regions extending over, at least, the smallest four wave vectors.

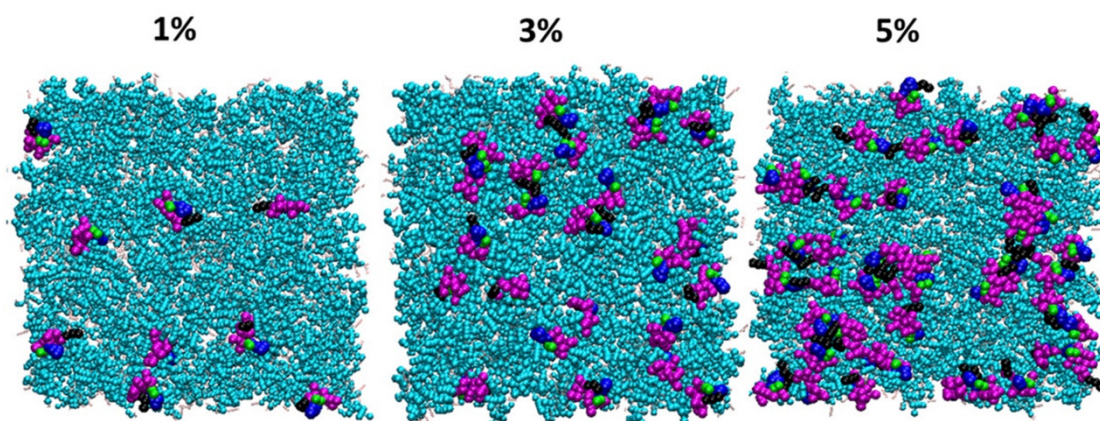


Figure S5. Top view of the snapshots of PmBs binding to the outer membrane model at different P/L ratios.